Journal of The Electrochemical Society, **162** (9) C503-C508 (2015)
0013-4651/2015/162(9)/C503/6/$33.00 © The Electrochemical Society

Ab-Initio Study of the Role of Mg_2Si and Al_2CuMg Phases in Electrochemical Corrosion of Al Alloys

Yi-Fa Qin[z] and Shao-Qing Wang

Shenyang National Laboratory for Materials Science, Institute of Metal Research, Chinese Academy of Sciences, Shenyang 110016, People's Republic of China

By using first-principles density-functional theory with generalized-gradient approximation, we calculate the work functions of various crystal planes of Mg_2Si and Al_2CuMg phases which are common in Al alloys. The correlation between work functions and the behavior of local corrosion for the two phases in Al alloys is explored. It is found that the work functions of the two phases are influenced significantly by the element termination on the surface. If Mg atoms are exposed to the outmost layer, both phases have low work functions (Φ) approaching pure Mg; else if terminating atoms are highly electronegative, for instance, Si atoms, the work functions are high. There is a huge gap between the maximum and minimum work functions for these phases due to the variety of surface terminations, consequently the Volta potential difference between Mg_2Si or Al_2CuMg particles and Al matrix could be positive or negative. As a result, particles of both phases could act as cathode or anode, or even reverse roles in Al alloy local corrosion.

Manuscript submitted April 24, 2015; revised manuscript received June 4, 2015. Published July 10, 2015.

Aluminum alloys are widely used for many applications in automotive, marine, aviation industries, etc., due to their low density, high strength and reasonable corrosion resistance. Copper, magnesium, zinc, silicon and lithium are often added to improve mechanical properties of aluminum alloys.[1,2] Intermetallic particles will be precipitated if the concentration of alloying elements reaches a particular level.[3,4] However, due to the galvanic interactions between intermetallic particles with Al matrix, local corrosion on Al alloys surfaces often initiates at the sites of intermetallic particles.[5–7]

The correlation between localized corrosion on Al alloys surface and intermetallic particles is an area of intense interest in recent years. As a technique derived from atomic force microscopy (AFM), scanning Kelvin force microscopy (SKPFM) has widely been used for ex situ investigations of galvanic interaction between intermetallic particles and matrix. Based on the findings of Schmutz and Frankel, there is a nearly linear correlation between corrosion potentials of pure metals and Volta potential differences (VPD) measured by SKPFM after immersion in neutral NaCl solution.[8] They also reported that, in the case of Al alloys, intermetallic particles possessed distinct Volta potential from the matrix. According to their findings, SKPFM has been used to characterize local surface electrochemical inhomogeneity and predict electrochemical behaviors of various intermetallic particles on alloys surfaces.[9–21]

Intermetallic particles with lower corrosion potential than the matrix dissolve prior to the surrounding matrix when the alloy is immersed in chloride-containing solution, and *vice versa*.[22] However, some intermetallic phases have complicated electrochemical behavior due to their incongruent dissolution of active elements. Mg_2Si and Al_2CuMg (S-phase) phases are the common strengthening phases in AA5xxx (Al-Mg-Si) and AA2xxx (Al-Mg-Cu) Al alloys, respectively. Both phases are more active than Al matrix in the early stage of immersion into chloride-containing solution. Following apparent selective dissolution of active elements, the potentials of the two phases shift toward the positive direction and exceed that of the surrounding matrix.[7,23–26] Consequently, the matrix around the Mg_2Si or Al_2CuMg (S-phase) particle remnants is attacked.

VPD measurements are usually but not always in agreement with the corrosion potential measurements that whether the intermetallic particles are nobler than the Al matrix or not. The Volta potential of the Mg_2Si phase is 100∼180 mV[5] and about 80 mV lower than Al matrix in AA7075 and AA5083 respectively.[23] By many publications, the corrosion potential of Mg_2Si is also negative relative to the Al matrix.[27] Birbilis and Buchheit reported that corrosion potential of synthetic bulk Al_2CuMg in NaCl solution (pH = 6,0.01 M,0.1 M, 0.6 M) is about 100∼300 mV lower than that of AA7075 matrix.[22] In contrast to the corrosion potential measured in NaCl solution by Birbilis and Buchheit, the Volta potential of Al_2CuMg could be more positive than that of Al matrix. Several values for the Volta potential of Al_2CuMg have been measured: 280 mV,[8] 150 mV,[28] and 20∼240 mV[18] higher than matrix in AA2024. The oxide layer on S-phase particles is considered as one of the reasons why S-phase particles are more active but possess more positive Volta potential than that of the Al matrix.[8] After removal of oxide layers with scratching or ion-etching, the previously noble Volta potential of S-phase particles shift toward levels similar to or even lower than that of the Al matrix.[25] The oxide layer thickness, chemical composition may lead to inaccurate reflection of Volta potential contrast. Since VPD measurement by SKPFM is implemented in air, it should be treated with caution if measured metals or alloys are prone to passivation.

SKPFM is a useful technique to investigate galvanic interaction between precipitated particles and matrix, and to predict electrochemical behaviors of intermetallic particles. However, the accuracy of SKPFM is disturbed by several factors, e.g. oxide film on intermetallic particles,[9] the spray capacity induced by the tip cantilever and surface terrain,[15] the size effect,[16] etc. By the experimental and theoretical analysis of McMurray and Williams,[16] VPD between the inclusion and the matrix would be underestimated if the size of inclusion is small compared to the sample-tip distance. All the factors above can be avoided by first-principles calculations since VPD is derived from the surface models without oxide film and protrusions. In this study, we carry out first-principles calculations to gain insight into the nature of selective dissolution of Mg_2Si and Al_2CuMg phases.

Theoretical Methods and Computational Details

Galvanic corrosion occurs when two different alloys are electrically connected and immersed in an aggressive electrolyte solution. The prerequisites of galvanic interaction are aggressive electrolyte solution and different corrosion potential of the two contacted alloys. Anodic polarization occurs to the alloy with a previously lower corrosion potential, consequently its corrosion is accelerated while the other alloy is protected. The potential difference could be regarded as the driving force of galvanic interaction while the aggressive electrolyte solution forms a loop of galvanic interaction. After removal of electrolyte solution, the driving force still remains in the form of Volta potential difference. This is the reason why VPD measurements are used to predict galvanic interaction between the matrix and intermetallic particles.

The Volta potential difference is defined by IUPAC as the electric potential difference between one point in the vacuum close to the surface of M1 and another point in the vacuum close to the surface of M2, where M1 and M2 are two uncharged metals brought into

[z]E-mail: yfqin10s@imr.ac.cn

contact.[29] SKPFM measures VPD ($\Delta\Psi$) between the intermetallic particles and the probe tip, or the matrix and the probe tip. According to Rohwerder, $\Delta\Psi$ equals the work function (Φ) difference between the sample and the tip:[15]

$$\psi_{IMP} - \psi_{probe} = \frac{1}{e}(\Phi_{IMP} - \Phi_{probe}) \quad [1a]$$

$$\psi_{matrix} - \psi_{probe} = \frac{1}{e}(\Phi_{matrix} - \Phi_{probe}) \quad [1b]$$

This enables to calculate VPD between the intermetallic particles and the matrix as follows:

$$\psi_{IMP} - \psi_{matrix} = \frac{1}{e}(\Phi_{IMP} - \Phi_{matrix}) \quad [2]$$

As the work function of the probe (Φ_{probe}) is a constant, the VPD measurement could be considered as a work function distribution map of the measured surface. Fortunately, the calculation of work function is straightforward with the density function theory method.[30]

Calculations were performed using the density functional theory (DFT)[31] as implemented in the Vienna Ab Initio Simulation Package (VASP)[32] with periodic boundary condition. The electron-ion interaction was described by the projector augmented plane wave method[33] with generalized gradient approximation (GGA). The Perdew-Burke-Ernzerh functional was applied to treat the electron exchange and correlation.[34] A plane-wave basis with an energy cutoff of 400 eV was used to expand electronic wave functions. For the calculation of the work function of an (hkl) surface, we adopt stoichiometric slab models with thickness 4 times as (hkl) interplanar spacing. The lower half of a slab model is fixed while the upper half is allowed to relax. A 15 Å vacuum layer was inserted along the direction of slab periodic repetition to minimize the surface–surface interaction. The convergence criterion for the slab structure optimization was set by a maximum Hellmann Feynman force tolerance of 0.03 eV/Å.

The work function was calculated as the difference between the vacuum level E_{vacuum} and the Fermi energy E_{Fermi}:

$$\Phi = E_{vacuum} - E_{Fermi} \quad [3]$$

The vacuum level and Fermi energy were obtained from the plane-averaged electrostatic potentials (Fig. 1a) and the output of DFT

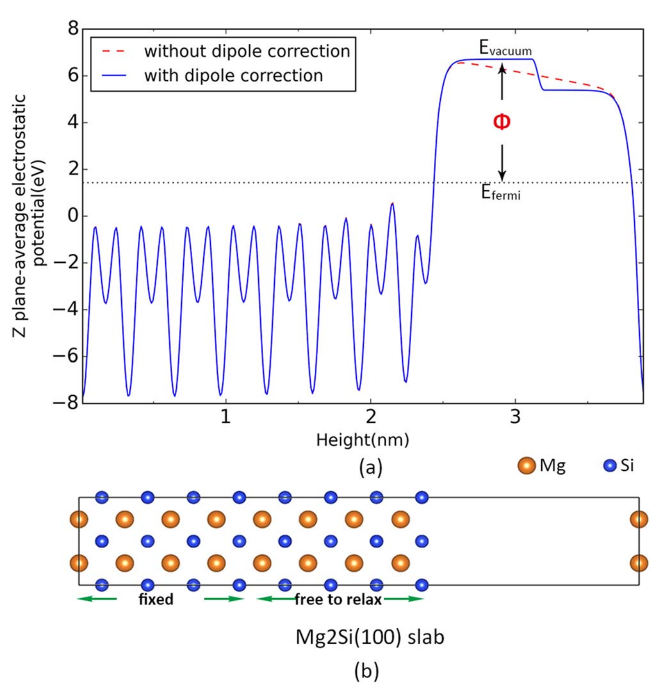

Figure 1. Plane-averaged electrostatic potential curve (a) of Si-terminated Mg_2Si (100) surface model (b).

Table I. Work functions of various surfaces of pure aluminum. Cal and Exp are from Refs. 43,44 respectively. Cal stands for calculated and Exp stands for experimental.

	(100)	(110)	(111)	(210)	(211)	Poly-crystalline
This work	4.29	4.04	4.09	4.32	4.21	-
Cal	4.30	4.09	4.02	-	-	-
Exp	4.20 ± 0.03	4.06 ± 0.03	4.26 ± 0.03	-	-	4.28 ± 0.01

ground-state calculation, respectively. Since the slabs are stoichiometric, the two surfaces of a slab are usually terminated with different elements. Dipole correction[35] was applied to eliminate the artificial electric field induced by different terminations of the two surfaces.

Results and Discussion

The work function of the Al matrix.— The matrix of commercial Al alloys contains many kinds of alloying elements and both the species and concentration of these elements can modify the work function of the Al matrix. Mg_2Si or Al_2CuMg phases are commonly found in the typical commercial Al alloys. The total weight fraction of alloying elements in Al alloys is usually lower than 10%. Moreover, the alloying elements preferably enrich in intermetallic particles, which leads to and even lower concentration of alloying elements in the Al matrix. We assume that the work function of commercial Al alloys approximately equals to that of pure aluminum. The calculated work functions of typical surfaces of pure Al are listed in Table I.

The calculated work function of Al ranges from 4.04 eV for the (110) surface to 4.32 eV for the (210) surface. The calculated result has a narrow scatter and is consistent with the experimental work function of polycrystalline Al, i.e. 4.28 eV. Data of (100), (110), (111) work functions show a good agreement with the theoretical and experimental literature as shown in Table I.

The work function of Mg_2Si phase.— Mg_2Si phase has cubic symmetry with space group Fm-3m[36] (Fig. 2). The optimized lattice constant is 6.357 Å, which matches experimental values 6.359 Å well.[37] Calculations were carried out for (100), (110), (111), (210), (211) surfaces and various atomic terminations. The results are listed in Table II.

The stacking along [100] of Mg_2Si phase can be described as a periodical sequence of an Mg-layer and an adjacent Si-layer, i.e. "…$Mg_ASi_AMg_BSi_B$…". Therefore, the (100) surface is either

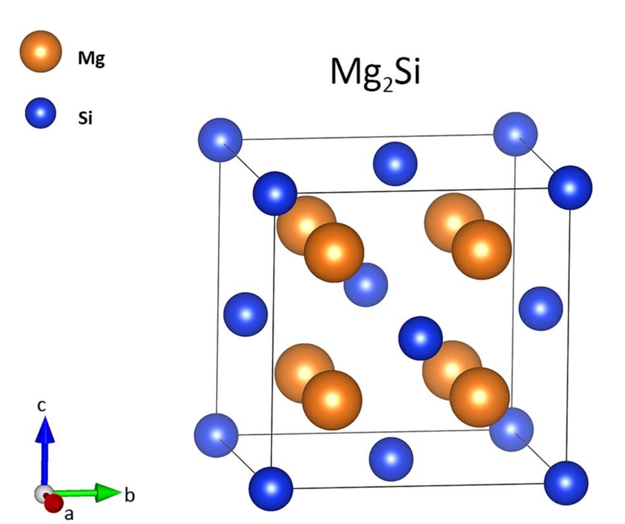

Figure 2. Schematic drawing of the Mg_2Si crystal structure.

Table II. Tabulated work functions of Mg_2Si and VPD between Mg_2Si and the Al matrix. The VPD values in the last column are calculated with respect to the experimental work function value of polycrystalline Al (4.28 eV).[44]

Surface	Terminated plane	Work function (eV)	VPD relative to the Al matrix (V)
(100)	Si	5.28	1.00
	Mg	3.94	−0.34
(111)	Si-Mg	5.24	0.96
	Mg-Mg	3.76	−0.52
	Mg-Si	3.02	−1.08
(210)	Si	4.64	0.36
	Mg	3.59	−0.69
(110)	Mix(Si,Mg)	3.72	−0.56
(211)	Mix(Si,Mg)	3.89	−0.39

terminated with Mg or Si atoms as shown Fig. 3. The work functions for Mg-terminated and Si-terminated (100) surfaces are 3.94 and 5.28 eV, respectively.

In the case of the (111) surface, the stacking of Mg_2Si can be described as "$\ldots Mg_A Mg_B Si \ldots$". Therefore, three terminations are possible for (111) surface, i.e. Si-Mg, or Mg-Mg, or Mg-Si, with work functions of 5.24, 3.76, 3.02 eV, respectively. The (111) surface models are presented in Fig. 4.

Mg_2Si (210) is a stepped surface with either Mg or Si atoms as the corner atoms (Fig. 5). The respective work functions are 3.59 and 4.64 eV. For (110) and (211) surfaces, the outmost layer is mixture of Mg and Si atoms with a ratio of 2:1 as shown in Fig. 6. Thus, both surfaces have only one termination type and the work functions are 3.72 eV for (110) and 3.89 eV for (211), respectively.

As shown in Table II, the work function of Mg_2Si ranges from 3.02 eV of Mg-Si-terminated (111) surface to 5.28 eV of Si-terminated (100) surface. A huge gap of 2.26 eV was found between the maximum and the minimum work functions of these calculated surfaces.

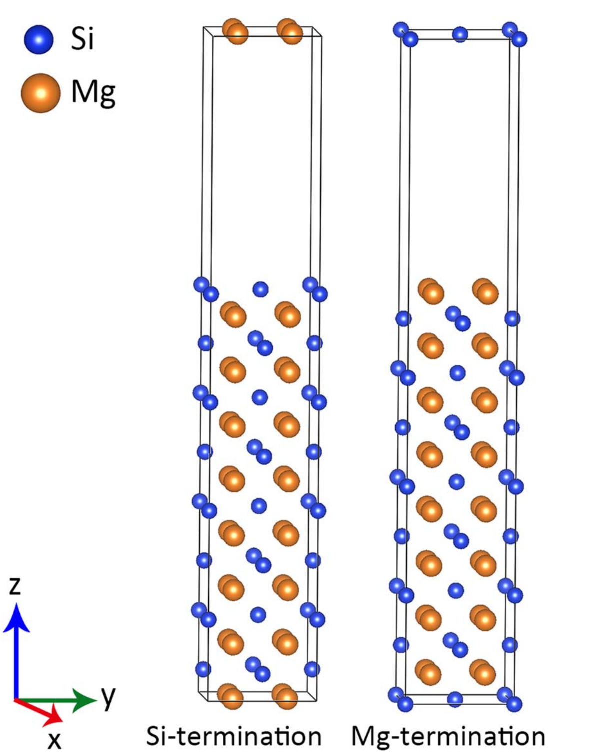

Figure 3. Mg_2Si (100) slab models. All two possible terminations are depicted.

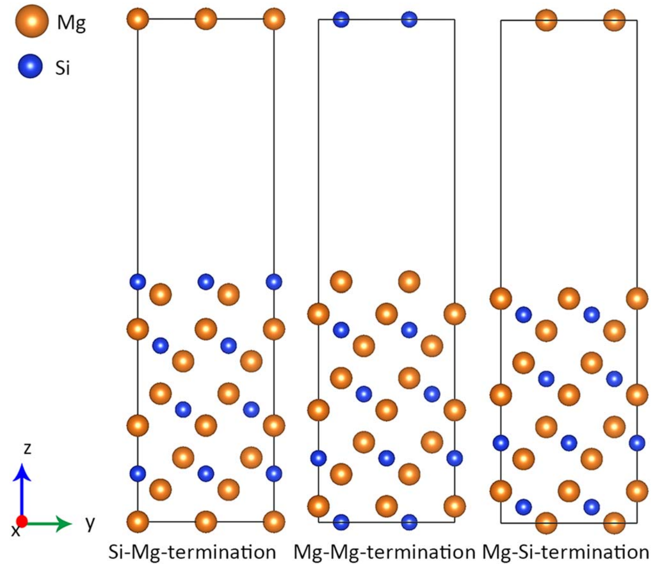

Figure 4. Mg2Si (111) slab models. All three possible terminations are depicted.

Interestingly, this gap is even larger than the one (1.19 eV) between the experimental values for pure silicon (4.85 eV) and magnesium (3.66 eV).[38] Unexpectedly, the minimum value 3.02 eV is 0.64 eV lower than the work function of polycrystalline magnesium. It can be summarized from the table that the species of terminated element have significant influence on the Mg_2Si work function. When the outermost layer contains Mg atoms only, the work function ranges from 3.02 to 3.94 eV, which is lower than that of pure Al. When Mg and Si atoms appear coplanar in the outermost layer, e.g. in the case of (110) and (211) surfaces, the work functions are lower than that of pure polycrystalline Al. Only when the surface is ended with Si atoms, the work function exceeds that of pure Al. It is obvious that Mg element is responsible for driving the work function to lower values, thus making these IMPs more anodic than the surrounding matrix.

The work function of Al_2CuMg.— Controversy arose over the crystal structure of Al_2CuMg (S phase) for decades and various models were suggested.[39–41] The model given by Perlitz and Westgren is widely accepted.[42] Here we adopt their model to carry out work

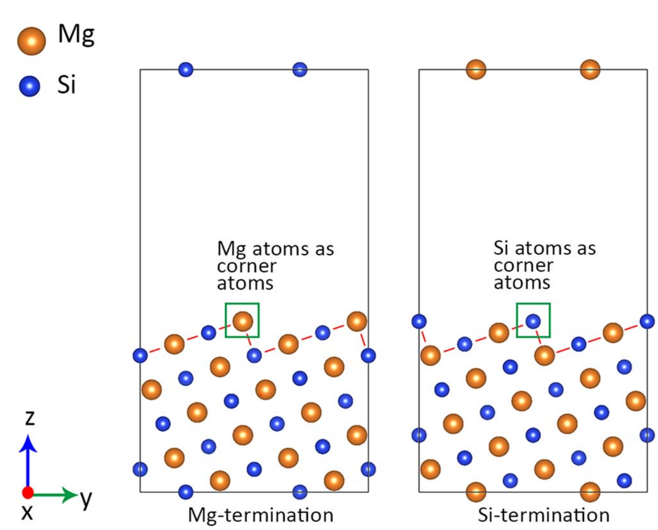

Figure 5. Mg_2Si (210) slab models. The surface steps are highlighted by red dashed lines. The atoms in rectangular box are atoms located at corner sites.

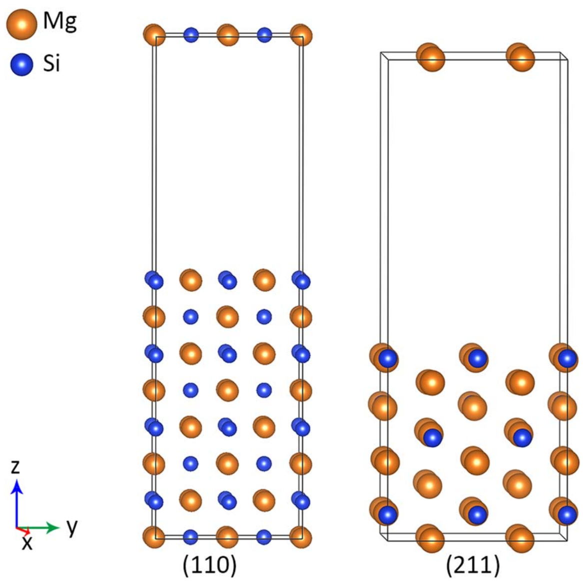

Figure 6. Mg_2Si (110) and (211) slab models.

function calculation of Al_2CuMg (Fig. 7). According to Perlitz and Westgren, Al_2CuMg is orthorhombic phase with space group Cmcm. Our optimized lattice constants of Al_2CuMg are a = 4.012 Å, b = 9.277 Å, c = 7.143 Å, which are in agreement with the experimental result: a = 4.00 Å, b = 9.23 Å, c = 7.14 Å. The unit cell contains 16 atoms in the ratio Al:Cu:Mg = 2:1:1.

Since Al_2CuMg contains three elements and has a complicated structure, Al_2CuMg surfaces have numerous terminations. The work functions of (001), (100), (010), (101), (130), (111) surfaces were calculated and are listed in Table III. There is only one termination for the (100) surface (Fig. 7), i.e. the outermost layer is a mixture of coplanar Al, Cu, Mg atoms. The corresponding work function is 4.34 eV. The stacking of Al_2CuMg (001) surface can be described as two adjacent Al layers and a mix layer of Cu and Mg atoms, i.e. "... Al_AAl_BMix..". Thus, three terminations of (001) surface are possible (Fig. 8), i.e. Al-Al-mix(Cu,Mg), mix(Cu,Mg)-Al-Al, Al-mix(Cu,Mg)-Al (the leftmost layer refers to the outermost layer). The corresponding work functions are 4.17, 4.28, 3.67 eV, respectively. There are also 3 terminations of (111) surface (Fig. 9), i.e. Al-Al-mix(Cu,Mg), mix(Cu,Mg)-Al-Al, Al-mix(Cu,Mg)-Al, for which the respective work functions are 4.15, 4.07, 3.81 eV. The case of (010) surface is complicated because there are six terminations (Fig. 10). For a (010) slab of Al_2CuMg, an Al layer is adjacent to a Cu layer or an Mg layer, an Cu layer is adjacent to another Cu layer or an Al layer, an Mg layer is adjacent to another Mg layer or an Al layer.

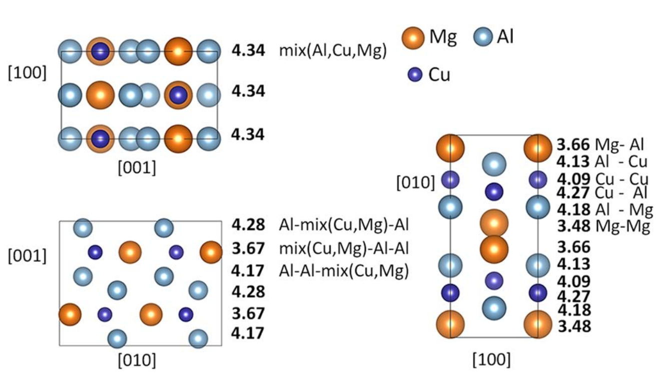

Figure 7. Schematic three view drawing of the S-phase crystal structure. Corresponding work functions are listed.

Table III. Tabulated work functions of Al_2CuMg and VPD between Al_2CuMg and the Al matrix. The VPD values are calculated with respect to the experimental value of polycrystalline Al.[44]

Surface	Terminated plane	Work function (eV)	VPD relative to the Al matrix (V)
(001)	Al-Al-Mix(Cu,Mg)	4.17	−0.11
	Mix(Cu,Mg)-Al-Al	3.67	−0.61
	Al-Mix(Cu,Mg)-Al	4.28	0.00
(100)	Mix(Al,Cu,Mg)	4.34	0.06
(010)	Mg-Mg	3.48	−0.80
	Al-Mg	4.18	−0.10
	Cu-Al	4.27	−0.01
	Cu-Cu	4.09	−0.19
	Al-Cu	4.13	−0.15
	Mg-Al	3.66	−0.62
(101)	Al-Al-Mix(Cu,Mg)	4.15	−0.09
	Mix(Cu,Mg)-Al-Al	3.81	−0.47
	Al-Mix(Cu,Mg)-Al	4.07	−0.21
(130)		3.79∼4.07	−0.49∼−0.11
(111)		3.74∼4.31	−0.54∼+0.03

Thus, the six terminations of (010) surface are Mg-Mg, Al-Mg, Cu-Al, Cu-Cu, Al-Cu, Mg-Al. When Mg atoms fully occupy the outermost and sub-outermost layers, the work function reaches a very low value of 3.48 eV. Mg-Al-terminated (010) surface has a little higher work function, which is 3.66 eV. When Al or noble Cu layer serves as the outermost layer, the work function falls in a narrow scatter, which is from 4.09 to 4.28 eV. Terminations of (130) and (111) surfaces are not shown for clarity due to their irregularity. The work function scatters of (130) and (111) are 3.79∼4.07 and 3.74∼4.31 eV respectively.

Correlation between work functions of Mg_2Si or Al_2CuMg and electrochemical behavior.— The range of the Mg_2Si work function is from 3.02 eV to 5.28 eV for calculated surfaces. The lower limit is well below while the upper limit is far beyond the work function of Al matrix (4.28 eV). Providing Mg atoms are present at the outermost

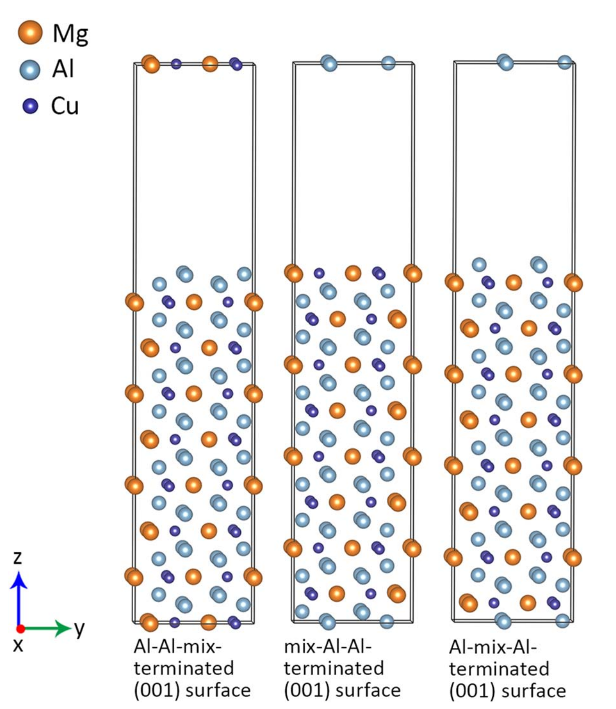

Figure 8. Al_2CuMg (001) slab models. All possible terminations are depicted.

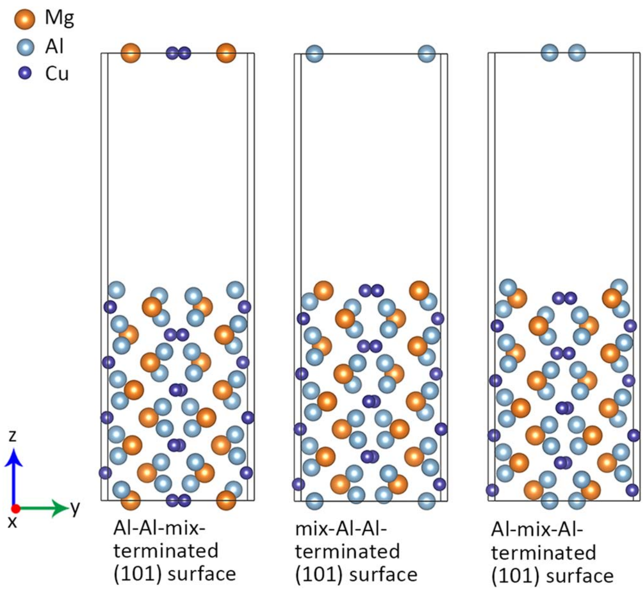

Figure 9. Al_2CuMg (101) slab models. All possible terminations are depicted.

layer, even mixed with Si atoms, the work functions of Mg_2Si drop to a level lower than the Al matrix ϕ. Only those surfaces terminated with a monolayer of silicon atoms possess high ϕ. Thus, ϕ of Mg_2Si is basically dominated by Mg element. From Eq. 2, it can be concluded that Mg_2Si particles generally have much lower Volta potentials than that of the Al matrix. This is in good agreement with the fact that the corrosion potential of synthetic bulk Mg_2Si is usually 700∼900 mV lower than that of the Al matrix.[22] Mg-terminated Mg_2Si particles have much lower Volta potential relative to the Al matrix and Si-terminated particles, therefore the galvanic interactions between anodes and cathodes are strong. As Mg atoms dissolve from Mg-terminated particles, the surfaces of particles become Si-rich. Thus, the potentials shift to a high level and the remnants of Mg_2Si particles transform from anodes to cathodes. This explains why Mg_2Si particles usually do not dissolve in entirety, i.e. Mg dissolves selectively and the remnants are porous and Si-rich. The huge gap between work functions of various terminations is responsible for selective dissolution and polarity inversion of Mg_2Si.

The range of Φ of Al_2CuMg is from 3.48 to 4.34 eV for calculated surfaces which is basically below the polycrystalline Al work function, 4.28 eV. Mg-rich surfaces possess work functions close to that of pure

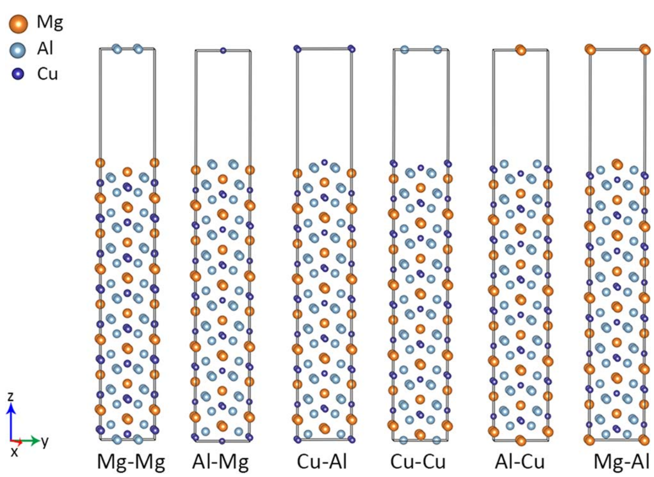

Figure 10. Al_2CuMg (010) slab models. All six possible terminations are depicted.

magnesium, 3.66 eV, while the work functions of Cu-rich and Al-rich surfaces are at the same level as pure aluminum, 4.28 eV. S phase Φ is basically dominated by Al and Mg elements. Mg atoms present at surfaces can drag down the work function of Al_2CuMg significantly. The Volta potentials of S phase particles are close to or lower than that of the Al matrix. It is in agreement with the fact that the corrosion potential synthetic bulk Al_2CuMg is lower than that of the Al matrix. Similar to Mg_2Si phase, Al_2CuMg particles with Mg-rich surfaces serve as anodes and start to dissolve when Al alloys are immersed in chloride-containing media. As the content of Mg decreases and the content of Cu increases, the S phase remnants transform from anodes to cathodes due to potential shift toward positive direction. In addition, the surfaces which are not terminated with Mg atoms share nearly the same potential level as the Al matrix. This is consistent with the facts that some S phase particles and the Al matrix around them remain nearly inert after immersion into NaCl solution.

In general, the alloy surface is composed of the matrix and the embedded intermetallic particles. The Volta potentials of Mg_2Si or Al_2CuMg may fall in a wide range due to their various exposed crystal planes and terminations. The inhomogeneous Volta potential distribution of Al surface corresponds to fluctuation of surface corrosion resistance. As shown above, Mg atoms present at surfaces significantly drag down work functions of the two phase particles, in other words, Mg-terminated particles are low-potential sites which usually serve as local attack initiation points. As corrosion goes on, surfaces of the two phases enrich with noble elements like Si and Cu, and the Volta potential map of the alloy surface is reshaped. Thus, local electrochemical behaviors on Al surfaces are complicated by redistribution of the potential map.

The surfaces we simulated are clean and unoxidized, while oxide films or adlayers will be present on real alloy surfaces. The analysis above is based on the assumption that oxide films are absent. The presence of oxidation states might also be contributing to the observed experimental results. Since we calculated the VPD between the two phases and the Al matrix in the absence of oxide films, the impact of oxidation to VPD or work function can be partially derived from combination of experiment results and calculation data.

Conclusions

By investigating correlation between Volta potential difference or work function and local electrochemical corrosion behaviors of Mg_2Si and Al_2CuMg phases, several conclusions can be drawn as follows:

(1) The validity of density functional theory method for research of galvanic interaction on Al alloy surface is demonstrated.
(2) Volta potential or work function of the two phases is highly sensitive to surface termination and composition. In particular, surface Mg atoms significantly drag down work functions toward pure magnesium ϕ.
(3) The huge gap between upper and lower limits of work function due to various surfaces and terminations is responsible for selective dissolution and polarity inversion of Mg_2Si and Al_2CuMg phases.
(4) Statistical analysis should be applied when VPD measurement is performed by SKPFM due to the wide scatter range of Volta potentials of intermetallic particles.

This article does not involve the impact of oxide films or hydroxide species toward surface properties like work function and their roles in Al alloys local corrosion, they will be discussed in future work.

Acknowledgment

The work described in this article was funded by the National Basic Research Program of China (973) (No.2011CB606403). The computational support from the Informalization Construction Project of Chinese Academy of Sciences during the 11th Five-Year Plan Period (no. INFO-115-B01) is also highly acknowledged.

References

1. N. Q. Chinh, J. Lendvai, D. H. Ping, and K. Hono, *J. Alloy. Compd.*, **378**, 52 (2004).
2. R. K. Gupta, N. Nayan, G. Nagasireesha, and S. C. Sharma, *Mater. Sci. Eng. A-Struct. Mater. Prop. Microstruct. Process.*, **420**, 228 (2006).
3. H. Okamoto, *Desk Handbook: Phase Diagrams For Binary Alloys*, p. 29, ASM International, Materials Park, Ohio (2000).
4. P. Villars, A. Prince, and H. Okamoto, *Handbook Of Ternary Alloy Phase Diagrams*, p. 3237, ASM International, Materials Park, Ohio (1997).
5. F. Andreatta, H. Terryn, and J. H. W. de Wit, *Corros. Sci.*, **45**, 1733 (2003).
6. N. Birbilis, M. K. Cavanaugh, and R. G. Buchheit, *Corros. Sci.*, **48**, 4202 (2006).
7. J. Wloka, G. Buerklin, and S. Virtanen, *Electrochim. Acta*, **53**, 2055 (2007).
8. P. Schmutz and G. S. Frankel, *J. Electrochem. Soc.*, **145**, 2285 (1998).
9. V. Guillaumin, P. Schmutz, and G. S. Frankel, *J. Electrochem. Soc.*, **148**, B163 (2001).
10. M. Rohwerder, E. Hornung, and M. Stratmann, *Electrochim. Acta*, **48**, 1235 (2003).
11. F. Andreatta, H. Terryn, and J. H. W. de Wit, *Electrochim. Acta*, **49**, 2851 (2004).
12. J. H. W. de Wit, *Electrochim. Acta*, **49**, 2841 (2004).
13. M. Jonsson, D. Thierry, and N. LeBozec, *Corros. Sci.*, **48**, 1193 (2006).
14. A. Davoodi, J. Pan, C. Leygraf, and S. Norgren, *Electrochim. Acta*, **52**, 7697 (2007).
15. M. Rohwerder and F. Turcu, *Electrochim. Acta*, **53**, 290 (2007).
16. H. N. McMurray and G. Williams, *J. Appl. Phys.*, **91**, 1673 (2002).
17. L. Lacroix, L. Ressier, C. Blanc, and G. Mankowski, *J. Electrochem. Soc.*, **155**, C131 (2008).
18. L. Lacroix, L. Ressier, C. Blanc, and G. Mankowski, *J. Electrochem. Soc.*, **155**, C8 (2008).
19. M. S. Xue, J. Xie, W. Li, C. G. Yang, Y. L. Ai, F. J. Wang, J. F. Ou, and J. P. Yao, *Physica B*, **406**, 4240 (2011).
20. C. Senoz, S. Borodin, M. Stratmann, and M. Rohwerder, *Corros. Sci.*, **58**, 307 (2012).
21. C. Senoz, A. Maljusch, M. Rohwerder, and W. Schuhmann, *Electroanalysis*, **24**, 239 (2012).
22. N. Birbilis and R. G. Buchheit, *J. Electrochem. Soc.*, **152**, B140 (2005).
23. K. A. Yasakau, M. L. Zheludkevich, S. V. Lamaka, and M. G. S. Ferreira, *Electrochim. Acta*, **52**, 7651 (2007).
24. V. Guillaumin and G. Mankowski, *Corros. Sci.*, **41**, 421 (1999).
25. P. Leblanc and G. S. Frankel, *J. Electrochem. Soc.*, **149**, B239 (2002).
26. G. O. Ilevbare, O. Schneider, R. G. Kelly, and J. R. Scully, *J. Electrochem. Soc.*, **151**, B453 (2004).
27. N. Birbilis and R. G. Buchheit, *J. Electrochem. Soc.*, **155**, C117 (2008).
28. T. H. Muster and A. E. Hughes, *J. Electrochem. Soc.*, **153**, B474 (2006).
29. *Compendium of Chemical Terminology Gold Book*, p. 327, International Union of Pure and Applied Chemistry (2014).
30. J. Wang and S.-Q. Wang, *Acta Phys. -Chim. Sin.*, **30**, 551 (2014).
31. W. Kohn and L. J. Sham, *Phys. Rev.*, **140**, 1133 (1965).
32. G. Kresse and J. Furthmuller, *Phys. Rev. B*, **54**, 11169 (1996).
33. P. E. Blochl, *Phys. Rev. B*, **50**, 17953 (1994).
34. J. P. Perdew, K. Burke, and M. Ernzerhof, *Phys. Rev. Lett.*, **77**, 3865 (1996).
35. J. Neugebauer and M. Scheffler, *Phys. Rev. B*, **46**, 16067 (1992).
36. H. Okamoto, *Desk Handbook: Phase Diagrams For Binary Alloys*, p. 553, ASM International, Materials Park, Ohio (2000).
37. C. R. Clark, C. Wright, C. Suryanarayana, E. G. Baburaj, and F. H. Froes, *Mater. Lett.*, **33**, 71 (1997).
38. D. R. Lide, *CRC Handbook of Chemistry and Physics*, Internet Version 2005, p. 2207, CRC Press, Boca Raton, FL (2005).
39. V. Radmilovic, R. Kilaas, U. Dahmen, and G. J. Shiflet, *Acta Mater.*, **47**, 3987 (1999).
40. Y. Jin, C. Z. Li, and M. G. Yan, *J. Mater. Sci. Lett.*, **9**, 421 (1990).
41. G. B. Winkelman, K. Raviprasad, and B. C. Muddle, *Acta Mater.*, **55**, 3213 (2007).
42. H. Perlitz and A. Westgren, *Ark. Kemi, Mineral. Geol.*, **16** (1943).
43. N. E. Singh-Miller and N. Marzari, *Phys. Rev. B*, **80** (2009).
44. R. M. Eastment and C. H. B. Mee, *J. Phys. F: Metal Phys.*, **3**, 1738 (1973).